Astronomy & Astrophysics manuscript no. Gradients
February 15, 2012

Metallicity Gradients in Disks

Do Galaxies Form Inside-Out?

K. Pilkington[1,2,3,⋆], C. G. Few[1,2,⋆], B. K. Gibson[1,2,3], F. Calura[1,4], L. Michel-Dansac[5], R. J. Thacker[2], M. Mollá[1,6], F. Matteucci[7], A. Rahimi[8], D. Kawata[8], C. Kobayashi[9], C. B. Brook[1,10], G. S. Stinson[1,11], H. M. P. Couchman[12], J. Bailin[13], and J. Wadsley[12]

[1] Jeremiah Horrocks Insitute, University of Central Lancashire, Preston, PR1 2HE, UK
e-mail: kpilkington@uclan.ac.uk e-mail: cgfew@uclan.ac.uk
[2] Department of Astronomy & Physics, Saint Mary's University, Halifax, Nova Scotia, B3H 3C3, Canada
[3] Monash Centre for Astrophysics, School of Mathematical Sciences, Monash University, Clayton, Victoria, 3800, Australia
[4] INAF, Osservatorio Astronomico di Bologna, via Ranzani 1, Bologna, 40127, Italy
[5] Centre de Recherche Astrophysique de Lyon, Université de Lyon, Université Lyon 1, Observatoire de Lyon, Ecole Normale Supérieure de Lyon, CNRS, UMR 5574, 9 avenue Charles André, Saint-Genis Laval, 69230, France
[6] Departamento de Investigación Básica, CIEMAT, Avda. Complutense 22, Madrid, E28040, Spain
[7] Departimento di Fisica, Sezione di Astronomia, Università di Trieste, via G.B. Tiepolo 11, 34131, Trieste, Italy
[8] Mullard Space Science Laboratory, University College London, Holmbury St. Mary, Dorking, Surrey, RH5 6NT, UK
[9] Centre for Astrophysics Research, University of Hertfordshire, Hatfield, AL10 9AB, UK
[10] Departamento de Física Teórica, Universidad Autónoma de Madrid, Cantoblanco, Madrid, E28049, Spain
[11] Max-Planck-Institut für Astronomie, Königstuhl 17, Heidelberg, 69117, Germany
[12] Department of Physics and Astronomy, McMaster University, Hamilton, Ontario, L8S 4M1, Canada
[13] Astronomy Department, University of Michigan, 500 Church St., Ann Arbor, MI, 48109-1042, USA

Preprint online version: February 15, 2012

ABSTRACT

Aims. We examine radial and vertical metallicity gradients using a suite of disk galaxy hydrodynamical simulations, supplemented with two classic chemical evolution approaches. We determine the rate of change of gradient slope and reconcile the differences existing between extant models and observations within the canonical "inside-out" disk growth paradigm.
Methods. A suite of 25 cosmological disks is used to examine the evolution of metallicity gradients; this consists of 19 galaxies selected from the RaDES (Ramses Disk Environment Study) sample (Few et al., in prep), realised with the adaptive mesh refinement code RAMSES, including eight drawn from the 'field' and six from 'loose group' environments. Four disks are selected from the MUGS (McMaster Unbiased Galaxy Simulations) sample (Stinson et al. 2010), generated with the smoothed particle hydrodynamics (SPH) code GASOLINE, alongside disks from Rahimi et al. (2011: GCD+) and Kobayashi & Nakasato (2011: GRAPE-SPH). Two chemical evolution models of inside-out disk growth (Chiappini et al. 2001; Mollá & Díaz 2005) were employed to contrast the temporal evolution of their radial gradients with those of the simulations.
Results. We first show that generically flatter gradients are observed at redshift zero when comparing older stars with those forming today, consistent with expectations of kinematically hot simulations, but counter to that observed in the Milky Way. The vertical abundance gradients at ∼1−3 disk scalelengths are comparable to those observed in the thick disk of the Milky Way, but significantly shallower than those seen in the thin disk. Most importantly, we find that systematic differences exist between the predicted evolution of radial abundance gradients in the RaDES and chemical evolution models, compared with the MUGS sample; specifically, the MUGS simulations are systematically steeper at high-redshift, and present much more rapid evolution in their gradients.
Conclusions. We find that the majority of the models predict radial gradients today which are consistent with those observed in late-type disks, but they evolve to this self-similarity in different fashions, despite each adhering to classical 'inside-out' growth. We find that radial dependence of the efficiency with which stars form as a function of time drives the differences seen in the gradients; systematic differences in the sub-grid physics between the various codes are responsible for setting these gradients. Recent, albeit limited, data at redshift $z\sim1.5$ are consistent with the steeper gradients seen in our SPH sample, suggesting a modest revision of the classical chemical evolution models may be required.

Key words. galaxies: abundances – galaxies: evolution – galaxies: formation – Galaxy: disc

1. Introduction

The recognition that metals are not distributed homogeneously throughout the disk of the Milky Way (Shaver et al. 1983) has proven to be fundamental in our efforts to understand the role of interactions, mergers, accretion, migration, and gas flows, in shaping the formation and evolution of galaxies. A rich literature now exists which confirms these radial abundance trends in both spirals (e.g. Simpson et al. 1995; Afflerbach et al. 1997; Mollá et al. 1999; Carrera et al. 2008; Kewley et al. 2010; Sánchez-Blázquez et al. 2011) and ellipticals (e.g. Kormendy & Djorgovski 1989; Franx & Illingworth 1990; Peletier et al. 1990). Vertical trends have been studied somewhat less frequently (e.g. Marsakov & Borkova 2005, 2006; Soubiran et al. 2008; Navarro et al. 2011), but provide

⋆ These authors contributed equally to this work.

unique insights into the discrete nature (or lack thereof) of the thin disk – thick disk interface (and associated kinematical heating processes).

Observations of nearby spiral galaxies show that the inner disks have higher metallicities than their associated outer disk regions; at the present day, typical gradients of ∼−0.05 dex/kpc are encountered. These somewhat shallow gradients have provided *critical* constraints on models of galaxy formation and evolution, and are fundamental to the predictions of the classical "inside-out" paradigm for disk growth. Predictions have been made of the time evolution of metallicity gradients in chemical evolution models (e.g. Mollá et al. 1997; Fu et al. 2009) and observationally from plantetary nebulae (e.g. Maciel et al. 2003), although until recently, we have had essentially no *direct* observational constraints on what the magnitude of the time evolution of the gradients should be. This has changed with the work of Cresci et al. (2010), Jones et al. (2010), Queyrel et al. (2011), and Yuan et al. (2011), who have, for the first time, extended radial abundance gradient work to high redshifts. Yuan et al. (2011) show that for at least one "Grand Design" disk at redshift z∼1.5, the metallicity gradient is significantly steeper (−0.16 dex/kpc) than the typical gradient encountered today.[1] Constraining the metallicity gradients of galaxies beyond the local Universe remains a challenge for the future.

Using SPH simulations of disk galaxy mergers, Rupke et al. (2010a) show strong correlations of metallicity with environment and merger history, focussing on the effects of gas inflows and star formation rate. Observations by Cooper et al. (2008) show that higher metallicity galaxies are more abundant in group enviroments and Kewley et al. (2006) showed that interacting pairs of galaxies have systematically lower metallicities (∼0.2 dex lower) than field galaxies or more loosely associated pairs. Radial gradients have been shown to flatten for galaxies that have experienced recent mergers (Kewley et al. 2010); these also result in higher velocity dispersions and redistribution of the cold gas. In agreement with this, Michel-Dansac et al. (2008) studied the mass-metallicity relation for merging galaxies and concluded that the infall of metal poor gas during merger events lowers the gas phase metallicity. However, the timescale over which redistributed gas develops into a gradient like those we see in spiral galaxies today is unknown.

There have been several studies of chemistry within cosmological hydrodynamical simulations (e.g. Raiteri et al. 1996b; Kawata & Gibson 2003; Okamoto et al. 2008; Scannapieco et al. 2008; Zolotov et al. 2010; Rahimi et al. 2010; Wiersma et al. 2011; Kobayashi & Nakasato 2011), each modelling certain observational properties with varying degrees of success. Some studies have examined the radial and/or vertical gradients using hydrodynamical codes (e.g. Rupke et al. 2010a; Rahimi et al. 2011), but the numerical study of radial gradients has predominantly been in the context of classical galactic chemical evolution codes (e.g. Prantzos & Boissier 2000; Chiappini et al. 2001; Mollá & Díaz 2005). In this paper, we use 25 simulations realised with three different cosmological hydrodynamical codes: GASOLINE (Wadsley et al. 2004) and GCD+ (Kawata & Gibson 2003), both gravitational N-Body + Smoothed Particle Hydrodynamic (SPH) (Monaghan 1992) codes, and RAMSES (Teyssier 2002), an Adaptive Mesh Refinment (AMR) code. Alongside these, we use the results from the chemical evolution models of Chiappini et al. (2001) and Mollá & Díaz (2005).

Our work aims to fill an important gap in the field, by complementing orbital parameter studies (e.g. Rupke et al. 2010a; Perez et al. 2011), systematic sub-grid physics parameter studies (e.g. Wiersma et al. 2011), and detailed dissections of individual systems (e.g. Rahimi et al. 2011; Zolotov et al. 2010; Kobayashi & Nakasato 2011), with a statistical sample of Milky Way-like analogs. Our approach is different, but complementary, to the careful and compelling parameter study of Wiersma et al. (2011); their, the goal was to vary the input physics and examine the outcome, regardless of whether or not the simulated end-products might be classified still as Milky Way-like. Instead, we have sampled a range of codes, sub-grid physics, and initial conditions, each of which has been 'calibrated', in some sense, by their respective authors, to resemble a classical Milky Way-like system. With that calibrated sample, our unique contribution is to examine the 'path' by which the gradients evolve, search for both random and systematic trends/differences between the samples, and compare with new empirical data at high-redshift.[2] *This is the first time such a comparison of the temporal evolution of metallicity gradients has been undertaken with a statistical sample of simulated disk galaxies.*

The outline of the paper is as follows. The main differences between the codes are described in §2, where we concentrate primarily upon the relevant mechanisms associated with the treatment of star formation and feedback (both energetic and chemical). The metallicity gradients inferred today for stellar populations of different ages are presented in §3. This is expanded upon in §4 where the radial metallicity gradients of the young stellar population as a function of redshift are considered. Finally, we summarise our findings in §5.

2. Simulations

The simulations used in this paper are fully described in Stinson et al. (2010: MUGS), Rahimi et al. (2011: Gal1), Kobayashi & Nakasato (2011: KN11) and Few et al. (in prep: RaDES); the main characteristics of the simulations and their parent codes are described here and itemised in Table 1. The chemical evolution models are fully described in Chiappini et al. (2001) and Mollá & Díaz (2005), but again we describe the main aspects in the following section.

[1] At even higher redshifts (z∼3.3), Cresci et al. (2010) and Troncoso et al. (2012, in prep), as part of the AMAZE/LSD surveys, suggest that *both* inverted gradients (higher abundances in the outskirts, relative to the inner disk) *and* standard declining gradients are seen. From the latter surveys, inverted gradients (ranging from +0.0 to +0.1 dex/kpc) appear associated with very massive stellar disks at these high-redshifts ($M_*>3\times10^9$ $M_\odot$), while declining gradients (ranging from −0.0 to −0.2 dex/kpc) appear associated with lower mass stellar disks ($M_*<3\times10^9$ $M_\odot$). Cresci et al. (2010) suggest that the inverted gradients are due perhaps to recent infall of pristine material into the inner disk. These Lyman Break Galaxies, with their ∼1−2 orders of magnitude greater star formation rates (relative to the typical Milky Way progenitor at that redshift), are more likely associated with massive spheroids in clusters/groups today (e.g. Nagamine 2002), as opposed to the Milky Way, and so are not directly comparable with the simulations described here.

[2] In spirit, this is exactly the approach taken in the seminal Galactic Chemical Evolution Comparison Project (Tosi 1996), which examined the time evolution of classic chemical evolution models *calibrated* to the solar neighbourhood, in order to see where they differed 'away' from this calibrated boundary condtion.

Suite	Galaxy Galaxy	M_{Tot} ($10^{11}M_\odot$)	$M_{*,disk}$ ($10^{10}M_\odot$)	r_{disk} (kpc)	Environment	$d[Z_{*,all}]/dh$ (dex/kpc)	$d[Z_{*,young}]/dR$ (dex/kpc)
MUGS	g15784	14.0	5.9	3.2	Field	−0.06	−0.04
	g422	9.1	2.0	2.8	Field	−0.06	−0.08
	g1536	7.0	3.3	2.5	Field	−0.07	−0.05
	g24334	7.7	2.7	1.0	Field	−0.03	−0.19
GCD+	Gal1	8.8	4.1	2.7	Field	−0.04	−0.01
Grape-SPH	KN11	11.0	2.0	4.7	Field	−0.03	−0.04
RaDES	Castor	10.5	7.2	4.0	Loose Group	−0.17	−0.03
	Pollux	4.2	3.4	3.0	Loose Group	−0.06	−0.05
	Tyndareus	3.3	1.3	1.3	Loose Group	−0.02	−0.05
	Zeus	2.3	1.0	1.7	Loose Group	−0.07	−0.04
	Apollo	8.9	6.3	3.0	Loose Group	−0.04	−0.06
	Artemis	7.5	3.2	1.9	Loose Group	−0.08	−0.05
	Daphne	3.1	2.1	2.7	Loose Group	−0.03	−0.06
	Leto	2.5	1.2	1.8	Loose Group	−0.04	−0.05
	Luke	11.3	6.6	5.4	Loose Group	−0.01	−0.03
	Leia	3.9	3.0	4.1	Loose Group	−0.05	−0.02
	Tethys	7.2	5.1	2.8	Field	−0.08	−0.05
	Krios	5.7	4.0	2.5	Field	−0.10	−0.05
	Atlas	6.5	4.4	2.8	Field	−0.06	−0.04
	Hyperion	10.0	7.7	3.6	Field	−0.07	−0.04
	Eos	4.6	2.5	2.0	Field	−0.19	−0.07
	Helios	10.5	6.6	1.6	Field	−0.11	−0.04
	Selene	6.1	5.2	3.5	Field	−0.05	−0.06
	Oceanus	11.0	10.0	6.6	Field	−0.03	−0.03
	Ben	7.7	4.2	3.9	Field	−0.04	−0.03

Table 1. Basic present-day (z=0) characteristics of the 25 simulated disks. Column (1): simulation suite to which the the code used to simulate the galaxy (Column (2)) belongs; Column (3): total (dynamical) mass within the virial radius; Column (4): mass of the stellar disk, after application of the kinematic and spatial cuts described in § 3; Column (5): exponential scalelength of the stellar disk; Column (6): local environment of the galaxy; Column (7): mass-weighted vertical stellar abundance gradient, averaged over the radial range $1.5<r_{\rm disk}2.5$; Column (8): mass-weighted radial *young* (stars born within the past 100 Myrs) stellar abundance gradient, after application of the kinematic and spatial cuts described in § 3.

2.1. MUGS

The MUGS galaxies were run using the gravitational N-body + SPH code GASOLINE which was introduced and described in Wadsley et al. (2004). Below, we emphasise the the main points concerning the star formation and feedback sub-grid physics used to generate this suite of simulations, but first remind the reader of the background framework in which they were evolved, in addition to their basic characteristics.

The MUGS sample (Stinson et al. 2010) consists of 16 galaxies randomly drawn from a cosmological volume $50h^{-1}$ Mpc on a side, evolved in a Wilkinson Microwave Anisotropy Probe Three (WMAP3) ΛCDM cosmology with H_0 = 73 km s^{-1} Mpc^{-1}, Ω_m = 0.24, Ω_Λ = 0.76, Ω_b = 0.04, and σ_8 = 0.76. Each galaxy is resimulated at high resolution by using the volume renormalization technique (Klypin et al. 2001), with a gravitational softening length of 310 pc. The galaxies range in mass from 5×10^{11} $M_\odot$ to 2×10^{12} $M_\odot$. The four galaxies with the most prominent disks[3] were selected: g422[4], g1536, g24334, and g15784, the latter of which is the closest to a Milky Way analog in the sample.

Star formation and supernovae feedback uses the blastwave model (Stinson et al. 2006) whereby gas particles can form stars when they are sufficiently dense (>1 cm^{-3}) and cool (<15000 K). Gas particles which satisfy these criteria can form stars according to the equation $\frac{dM_\star}{dt}=c^\star\frac{M_{gas}}{t_{dyn}}$, where $c^\star$ is the star formation efficiency and is fixed to be 0.05. M_{gas} is the mass of the gas particle forming the star particle of mass $M_\star$ and t_{dyn} is the dynamical time of the gas. Heating from a uniform ultraviolet ionising background radiation field (Haardt & Madau 1996) is employed, and cooling is derived from the contributions of both primordial gas and metals; the metal cooling grid is derived using CLOUDY (v.07.02: Ferland et al. (1998)), under the assumption of ionisation of equilibrium, as detailed by Shen et al. (2010).

The chemical evolution model used in GASOLINE is fully described in Raiteri et al. (1996a); here, we only discuss the main points. All stars with masses above 8 $M_\odot$ explode as Type II supernova (SNeII). An efficiency factor couples 40% of a given supernova's energy (10^{51} erg) to the surrounding interstellar medium (ISM). The metals that are tracked in this version of GASOLINE (O and Fe) all come from supernovae and are allowed to diffuse between neighbouring SPH particles, after Shen et al. (2010). The Type Ia supernovae (SNeIa) eject iron and oxygen; for every SNIa, 0.76 $M_\odot$ of 'metals' is ejected, divided between iron (0.63 $M_\odot$) and oxygen (0.13 $M_\odot$). Our binary model for Type Ia supernovae is based upon the single-degenerate progenitor formalism of Greggio & Renzini (1983), with secondaries spanning in mass from 1.5 to 8.0 $M_\odot$.[5] Enrichment from SNeII

[3] By 'prominent', we mean the inclusion of those for which there was unequivocal identification of the disk (from angular momentum arguments constructed from the gas and young star distributions, as discussed in §3.1. In a secondary sense, this eliminated extreme values of bulge-to-total, but formally, we only included those disks for which alignment based upon the gas/young stars was obvious.

[4] g422 was not described in the original MUGS paper (Stinson et al. 2010); it was produced identically to the MUGS suite and will be described fully in an upcoming paper.

[5] We have excluded secondaries in the 0.8 - 1.5 $M_\odot$ range; doing so, regardless of IMF, only impacts on the SNeIa rate at the ∼20% level.

is based upon power law fits in stellar mass to the nucleosynthesis yield tables of Woosley & Weaver (1995), convolved with a Kroupa (Kroupa et al. 1993) initial mass function (IMF), in order to determine the mass fraction of metals ejected. The total metallicity in this version of the code is tracked by assuming Z≡O+Fe.[6] For these runs, only the $Z=Z_{\odot}$ yields were used, and long-lived SNeIa progenitors (those with secondaries with mass $m<1.5$ $M_{\odot}$) were neglected.

2.2. Gal1

Gal1 is a higher-resolution re-simulation of galaxy D1 from Kawata et al. (2004) using the SPH code GCD+ (Kawata & Gibson 2003); while its characteristics have been discussed previously by Bailin et al. (2005), Rahimi et al. (2010), and Rahimi et al. (2011), an overview is provided here for completeness. Employing a comparable volume renormalisation / 'zoom-style' technique to that described in § 2.1 (with a gravitational softening of 570 pc in the highest resolution region), Gal1 was realised within a ΛCDM cosmological framework with $H_0 = 70$ km s^{-1} Mpc^{-1}, $\Omega_m = 0.3$, $\Omega_\Lambda = 0.7$, $\Omega_b = 0.04$, and $\sigma_8 = 0.9$, resulting in a Milky Way analog of virial mass 8.8×10^{11} $M_{\odot}$. The effect of the ultraviolet background radiation field was neglected, while metal-dependent radiative cooling (adopted from MAPPINGS-III (Sutherland & Dopita 1993)) was included.

The star formation prescription employed requires (i) the gas density to be above a threshold of 0.1 cm^{-3}, (ii) a convergent gas flow to exist, and (iii) the gas to be locally Jeans unstable. A standard Salpeter initial mass function (IMF) was assumed, along with pure thermal feedback from both SNeII and SNeIa (10^{50} erg/SN) being coupled to the surrounding SPH particles.

The chemical evolution implementation within GCD+ takes into account the metal-dependent nucleosynthetic byproducts of SNeII (Woosley & Weaver 1995), SNeIa (Iwamoto et al. 1999), and low- and intermediate-mass AGB stars (van den Hoek & Groenewegen 1997). Relaxing the instantaneous recycling approximation, GCD+ tracks the temporal evolution of the nine dominant isotopes of H, He, C, N, O, Ne, Mg, Si, and Fe. The SNeIa progenitor formalism of Kobayashi et al. (2000) is adopted.

2.3. KN11

KN11 corresponds to the so-called 'Wider Region' model described by Kobayashi & Nakasato (2011), realized used a hybrid GRAPE-SPH code. This model was drawn from the 5 Milky Way-analogs which eventuated from a larger suite of 150 semi-cosmological[7] simulations. The cosmological parameters employed match those of §2.2, and led to a Milky Way analog of mass 1.1×10^{12} $M_{\odot}$. The effect of the ultraviolet background radiation field was included, as was metal-dependent radiative cooling (adopted from MAPPINGS-III (Sutherland & Dopita 1993)).

The star formation prescription employed requires (i) the gas density to be cooling, (ii) a convergent gas flow to exist, and (iii) the gas to be locally Jeans unstable. The star formation timescale is chosen to be proportional to the dynamical timescale ($t_{\rm sf}\equiv t_{\rm dyn}/c$), where the star formation efficiency is chosen to be c=0.1. A standard Salpeter initial mass function (IMF) was assumed (with lower and upper mass limits of 0.07 and 120 $M_{\odot}$, respectively), along with pure thermal feedback from both SNeII[8] and SNeIa ($\sim10^{51}$ erg/SN) being distributed to the surrounding SPH particles within 1 kpc (weighted by the SPH kernel).

The chemical evolution implementation within GRAPE-SPH takes into account the metal-dependent nucleosynthetic byproducts of SNeII (Kobayashi et al. 2006), SNeIa (Nomoto et al. 1997), and low- and intermediate-mass AGB stars (Karakas 2010).

2.4. RaDES

The third galaxy sample (RaDES: Ramses Disk Environment Study) was simulated using the adaptive mesh refinement (AMR) code RAMSES (Teyssier 2002). The motivation behind these simulations was to determine the systematic differences between simulated galaxies with neighbouring dark matter haloes similar to the Local Group and those in the field. The RAMSES simulations include gravity, radiative cooling, and heating from a uniform ionising UV background radiation (Haardt & Madau 1996). Hydrodynamic behaviour of the gas phase and gravitational potential is calculated on a spatially adaptive grid. A full description of the star formation model used in RAMSES is given by Dubois & Teyssier (2008); here we give just a brief account of its implementation.

Gas cells with density greater than a given threshold allow stars to form at a rate proportional to the density, $\dot{\rho} = -\rho/t_{\star}$, where $t_{\star}$ is the star formation timescale, which itself is proportional to the dynamical time ($t_0(\rho/\rho_0)^{-1/2}$), as first described by Rasera & Teyssier (2006). After Dubois & Teyssier (2008), we use a threshold of $\rho_0 = 0.1$ cm^{-3} and $t_0 = 8$ Gyr. In combination, these choices correspond to an adopted star formation efficiency of 2%. Feedback from SNeII[9] occurs instantaneously and the mass carried away is parameterised as ($\eta_{SN}+\eta_W$), where η_{SN} is the fraction of a stellar particle's mass that is ejected by SNeII and η_W is the fraction that is swept up in the SNII wind. In the RaDES simulations, $\eta_{SN} = 0.1$ and $\eta_W = 0$, which for these runs, led to less strongly peaked rotation curves. Energy is injected into the gas phase in the form of thermal and kinetic energy, distributed across a superbubble of radius $r_{\rm bubble}$ according to a Sedov blastwave formalism.The metallicity of SN ejecta is determined by converting a fixed fraction, f_Z, of the non-metal content of new stars into metals; all galaxies in the RaDES sample used f_Z=0.1.

RaDES is comprised of two subsamples allowing for a statistical intercomparison of field galaxies and those in environments similar to those of loose groups; the full details will be presented in Few et al. (in prep). These simulations take place

[6] By assuming Z=O+Fe, we admittedly underestimate the global metal production rate by nearly a factor of two; our next generation runs with GASOLINE employ a more detailed chemical evolution model, incorporating the nucleosynthetic byproducts of asymptotic giant branch evolution and thereby ameliorating this effect.

[7] By 'semi-cosmological', we mean that the simulated field was not large enough to sample the longest waves (and, as such, underestimate the degree of gravitational tidal torque which would otherwise be present in a fully cosmological framework), and so the initial system is provided with an initial angular momentum via the application of rigid rotation with a constant spin parameter λ=1.

[8] 50% of the massive stars are assumed to end their lives as SNeII, while the remaining 50% are assumed to end their lives as 10× more energetic hypernovae.

[9] SNIa are not accounted for in RaDES, although we have recently completed a chemical evolution upgrade to RAMSES which parallels that implemented within GCD+ (§ 2.2); this will described in a future work.

in either $20h^{-1}$ Mpc (grid resolution of 440 pc) or $24h^{-1}$ Mpc (grid resolution of 520 pc) volumes with 512^3 dark matter particles in the central region. The cosmology of these boxes is H_0=70 km $s^{-1}Mpc^{-1}$, Ω_Λ=0.72, Ω_m=0.28, Ω_b=0.045, and σ_8=0.8.

The sample employed here consists of nine isolated (field) galaxies and ten situated within loose groups. The latter are defined as being those for which two L_* halos of comparable mass reside within 1.5 Mpc of one another, and neither are located within 5 Mpc of a halo with mass in excess of 5×10^{12} $M_\odot$. The latter criterion avoids the proximity to rich clusters. In a statistical sense, these 'loose groups' can be thought of as Local Group analogs, at least in terms of dynamical mass, proximity to companion galaxies, and the avoidance of rich clusters. The field sample contains those halos that are even more isolated from neighbouring massive halos : specifically, no $M_{halo} > 3\times10^{11}$ $M_\odot$ within 3 Mpc). The virial mass range of the RaDES sample spans 2.5×10^{11} to 1.6×10^{12} $M_\odot$.

2.5. Chemical Evolution Models

In this work, we compare our results from the hydrodynamical simulations described in § 2.1–2.3 to two chemical evolution models both designed to reproduce the main features of our Galaxy. The models are described by Chiappini et al. (2001) and Mollá & Díaz (2005), and we refer the reader to these papers for full details.

In the model by Chiappini et al. (2001), the Milky Way forms by means of two main infall episodes, both represented by exponential infall rates. The first infall episode, characterised by the rate $\dot{\sigma_H} \propto A\ e^{-t/\tau_{inf,H}}$, is associated with the formation of the halo and thick disk, with an e-folding timescale ($\tau_{inf,H}$) of ∼1 Gyr. The constant A is determined by requiring that the present-day mass surface density of the halo is reproduced.

The second infall phase is represented as $\dot{\sigma_D} \propto B(R)\ e^{-t/\tau_{inf,D}}$, and is associated with the formation of the thin disk. The thin disk is represented by independent annuli, each 2 kpc wide, with no exchange of matter between them (i.e., no radial gas flows). The e-folding timescale ($\tau_{inf,D}$) of the second infall is assumed to be a linear function with increasing galactocentric radius (i.e., $\tau_{inf,D}(R) \propto R$) - enforcing the so-called "inside-out" paradigm for disk growth, with the gas accumulating faster in the inner regions of the disk, relative to the outer disk. The timescales here vary from ∼2 Gyr in the inner disk, to ∼7 Gyr in the solar neighbourhood, and up to ∼20 Gyr in the outermost parts of the disk. The constant $B(R)$ is fixed in order to reproduce the present-day total surface mass density (stars + gas) in the solar neighbourhood. The star formation rate $\dot{\sigma_*}$ is expressed by the common Schmidt-Kennicutt law, $\dot{\sigma_*} \propto \nu\sigma^k_{gas}(R,t)$, where $\sigma_{gas}(R,t)$ represents the gas density at the radius R and at the time t, and k = 1.5. The star formation efficiency ν is set to 1 Gyr^{-1}, and becomes zero when the gas surface density drops below a certain critical threshold, adopted here to be σ_{th}=7 $M_\odot\ pc^{-2}$. The nucleosynthesis prescriptions for AGB stars and SNeIa+SNeII are drawn from the same sources listed in § 2.2.

The chemical evolution model of Mollá & Díaz (2005) differs from that of Chiappini et al. (2001) in several aspects, in that it is multiphase, treating the ISM as a mixture of hot diffuse gas and cold molecular clouds. Each galaxy is assumed to be a two-zone system, comprised by a halo formed in an early gas-rich phase and a disk. The gas of the disk is acquired from the halo through an imposed infall prescription characterised by the inverse of the collapse time, which itself depends upon the total mass of the galaxy. The mass profile is imposed to adhere to the Persic et al. (1996) universal rotation curve. Similar to Chiappini et al. (2001), each galaxy is divided into concentric cylindrical zones 1 kpc wide. The collapse timescale depends on radius via an exponential function $\tau(R) \propto e^R$, rather than the linear dependence upon R employed by Chiappini et al. (2001). Another important difference concerns the treatment of star formation: in the Mollá & Díaz (2005) model, stars form in two stages: first, molecular clouds condense with some efficiency out of the diffuse gas reservoir, and second, stars form with a second efficiency factor based upon cloud-cloud collision timescales. In spirit, this mimics the effect of the threshold effect in the Chiappini et al. (2001) model: specifically, stars may form only in dense regions. The relation between the star formation rate and the gas density can be approximated by a power law with $n > 1$, again, in qualitative agreement with the law employed by Chiappini et al. (2001). In the halo, star formation follows a common Schmidt-Kennicutt law with exponent n = 1.5. Extensive testing and tuning of the main parameters resulted in a grid of 440 models spanning 44 different masses (from dwarfs to giants, with 10 different star formation efficiencies per mass model). The chemical prescriptions for SNeIa and SNeII are again similar to those listed in § 2.2.

3. Present-Day Gradients

3.1. Radial Gradients

In this section, the present-day radial abundance gradients of the MUGS and RaDES simulations are presented. We focus here on one MUGS (g15784) and one RaDES galaxy (Apollo), which have been chosen as fiducial representatives of these two suites of simulations. Observational constraints on the abundance gradient of z=0 late-type galaxies may be found in, for example, Zaritsky et al. (1994) who measured a mean gradient of −0.058 dex/kpc for local spiral galaxies and van Zee et al. (1998), who found a comparable mean gradient from their sample (−0.053 dex/kpc). In Kewley et al. (2010) close galaxy pairs were found to have systematically shallower gradients (typically, −0.021 dex/kpc). In each of these cases, the gradients are inferred from gas-phase nebular emission, which provides a "snapshot" of the present-day gradient, similar to that inferred from, for example, B-stars (i.e., stars with ages <100 Myrs).[10]

We employed a strict kinematic decomposition of spheroid and disk stars for each of the 25 simulations[11], following the Abadi et al. (2003) formalism. Additional (conservative) spatial cuts were employed to eliminate any satellite interlopers that might pass the initial kinematic decomposition. We define three age bins: young (stars born in the last 100 Myrs, to correspond roughly with B-stars), intermediate (stars formed 6−7 Gyr ago), and old (stars olders than 10 Gyr).

[10] Loose group galaxies in the RaDES suite exhibit the same qualitative flattening of metallicity gradients when compared with their 'field' equivalents, however the order of this difference is significantly smaller (<0.005 dex/kpc) than the systematic differences found between the RaDES and MUGS galaxies (∼0.05–0.2 dex/kpc). A comprehensive analysis of the (subtle) systematic differences between the field and loose group galaxies within RaDES is forthcoming (Few et al., in prep), but not pursued here, simply because this difference is negligible to the scope of the present analysis.

[11] The kinematic decomposition employed for the MUGS galaxies differs from that used in the original Stinson et al. (2010) analysis, in that J_z/J_{circ} for each star was derived self-consistently taking into account the shape of the potential, rather than assuming spherical symmetry and using the enclosed mass at a given star particle's position.

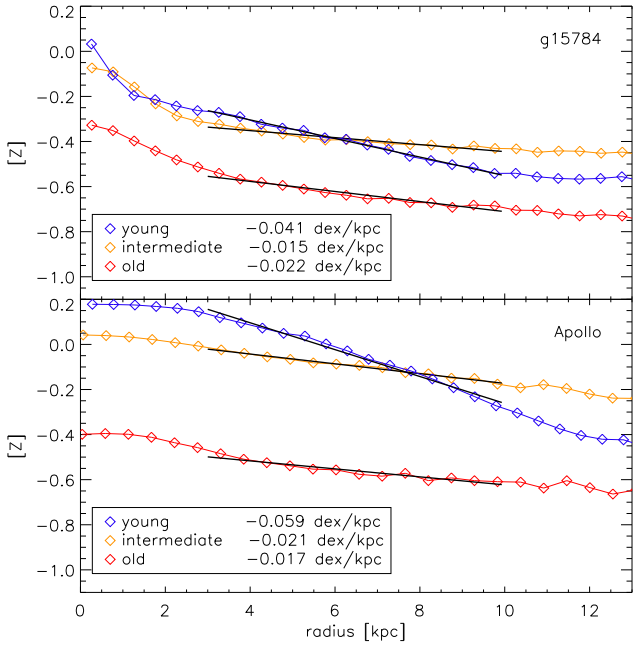

Fig. 1. Stellar radial [Z] gradients, for disk stars in three different stellar populations: young (blue) is defined as stars formed in the last 100 Myrs, intermediate (yellow) is defined as stars formed 6 to 7 Gyr ago, and old (red) is defined as stars older than 10 Gyr. Fits to the disk are overdrawn in black; the length of the black line corresponds to the region of the disk used in the fitting (see text for details). For clarity, only two galaxies are shown, one from MUGS (g15784, upper panel) and one from RaDES (Apollo, lower panel).

Observational studies of radial gradients typically show higher metallicities in the inner disk relative to the outer disk (e.g. Rupke et al. 2010b). As noted above, observations of external systems typically make use of gas-phase oxygen abundances, as measured from HII regions, but consistency exists between that tracer and others known to provide a "snapshot" of the gradient (e.g., planetary nebulae and short-lived main sequence B-stars). Our gas-phase and young (B-star) gradients are identical in amplitude and gradient, and hence in what follows, we employ "young stars" (those formed in the previous 100 Myr period) to determine the abundance gradients.

The current RaDES sample only tracks global metallicity Z, but as oxygen consistently accounts for ∼50% of Z, we use Z as a first-order proxy for oxygen, when making comparisions with observations.[12] The version of GASOLINE employed for these MUGS runs track both O and Fe (from SNeII and SNeIa), and assume Z≡O+Fe; as noted earlier, this latter assumption leads to an ∼0.2 dex underestimate of the global metallicity in the MUGS sample. This does not impact upon our gradient analysis, but does serve to explain why the RaDES and MUGS galaxies are offset by ∼0.2 dex from one another in [Z] in the figures presented here.

Figure 1 shows the mass-weighted radial gradients at z=0 in [Z] for one MUGS galaxy (g15784, top panel) and one RaDES galaxy (Apollo, lower panel). The radial gradients are calculated using linear fits over the noted disk regions (overdrawn in black). These are chosen to exclude the central region, avoiding any residual co-rotating bulge stars that escaped the kinematic decomposition. The outer edge of the disk is taken as the point at which the surface brightness profile of the young stars (effectively, the cold gas) deviates from an exponential. To ensure that an appropriate region is considered here, we have been conservative in choosing the "disk region". The gradient is robust to the choice of outer radius; reducing the choice of inner radius from 5 kpc to 2 kpc has only a ±0.007 dex/kpc impact on the inferred formal gradient - i.e., the differences in gradients between young, intermediate, and old populations are not significantly affected. Throughout this paper we use the Asplund et al. (2009) values for the solar metallicity.

As one considers progressively older stellar populations (at the present-day), Figure 1 shows that the measured radial metallicity gradient becomes progressively flatter. Such behaviour is not unexpected in cosmological simulations which include gas infall, radial flows, high velocity dispersion gas, kinematically hot disks, and dynamical mixing/radial migration which is more pronounced for older stars (e.g. Sánchez-Blázquez et al. 2009; **?**; Pilkington & Gibson 2012). The timescale of the mixing that flattens the gradients in the MUGS and RaDES simulations is shorter than the difference between intermediate and old populations of stars, as evidenced by radial gradients for the two populations, regardless of simulation suite, being quite similar. The degree of flattening of the *stellar* abundance gradients is such that by the present day, *within the simulations*, the older stellar tracers show a flatter abundance gradient than the younger tracers (recall Fig 1, re-iterating results shown by Sánchez-Blázquez et al. (2009), Rahimi et al. (2011), and Pilkington & Gibson (2012)). This is counter to what is observed in the Milky Way when inferring gradients using younger planetary nebulae versus older planetary nebulae (e.g. Maciel et al. 2003), but again, this is fully expected given the degree of kinematic (stellar) heating within these cosmological simulations, and does *not* impact on the use of gas-phase and young-star probes of the gradients (both possess the expected steeper abundance gradients at early-times).Indeed, future work in this area can, and should, make use of this powerful constraint on migration/heating: specifically, the fact that (empirically) older stellar probes today have a steeper abundance gradients than younger stellar probes, while extant, kinematically hot, simulations, show the opposite trend.

For completeness, in Table 1 we list the present-day mass-weighted stellar radial metallicity gradients (d[Z]/dR, in units of dex/kpc) for each of the 25 simulations employed here (column 8). The similarity of the gradients is readily apparent, save for the MUGS galaxy g24334, which was included in the sample despite its stellar fraction being dominated by accreted stars, rather than *in situ*star formation (discussed further in § 4). Its relatively small disk scalelength (1.0 kpc) also made fitting its gradient more challenging than the other MUGS disks.

Following Sánchez-Blázquez et al. (2011), we examined the effect of applying a different weighting scheme in determining the mean metallicities. When examining just the young stars or the gas, the weighting employed has no effect upon the inferred gradient. However, when deriving a composite gradient making use of *all* stars in the disk, the weighting can become important, as Sánchez-Blázquez et al. (2011) suggested. We explored the impact of using, for example, luminosity-weighting (and log-weighting), by deriving the absolute magnitude of each simulated star particle, making use of its age, metallicity, and initial

[12] We have recently completed the implementation of full chemical evolution, including SNeII, SNeIa, and AGB stars, within RAMSES - Few, Gibson & Courty (2011, in prep).

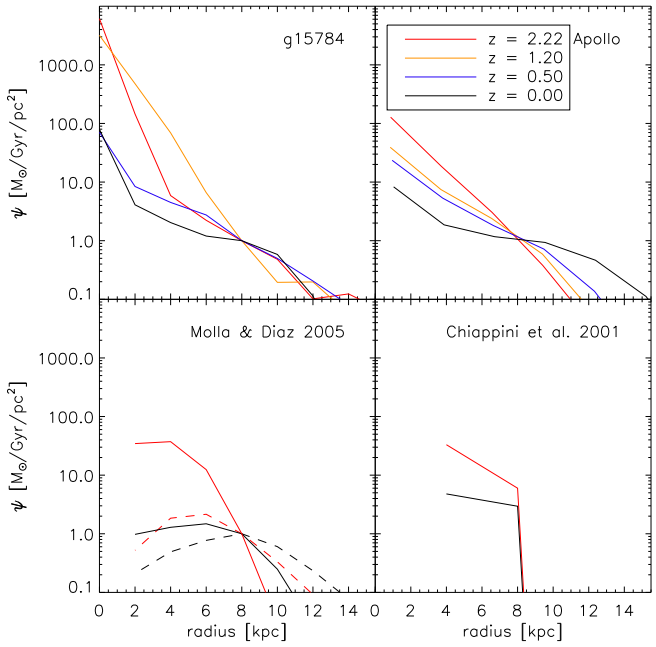

Fig. 2. Star formation rate per unit surface area as a function of radius for the MUGS galaxy g15784 (upper-left panel) and the RaDES galaxy Apollo (upper-right panel). We show the simulations at four different redshifts: z=0.0, 0.5, 1.2, and 2.2, as noted in the inset to the upper-right panel. 1 kpc annuli are used along with a height cut of ±5 kpc above and below the disk. The mass of stars formed in the last 100 Myrs is calculated for each annulus out to a radius of 15 kpc. The curves have been normalised to 1 $M_{\odot}$/Gyr/pc^2 at galactocentric radius 8 kpc. The bottom panels show the corresponding predicted behaviour of the Chiappini et al. (2001) (right) and Mollá & Díaz (2005) (left) models. Only redshifts 0.0 and 2.2 are shown, other redshifts are excluded as these models evolve smoothly from z=2.2 to z=0.0. Two of the Mollá & Díaz (2005) models are shown, one with high star formation efficiency (dashed lines) and one with low star formation efficiency (solid lines) .

mass function, alongside the Marigo et al. (2008) isochrones.[13] As expected from the Sánchez-Blázquez et al. (2011) analysis, the mean abundance shifted by ∼0.1 dex depending upon the weighting employed, but the inferred gradient was not affected.

The abundance gradient of young stars (or equivalently, the ISM) is shaped by the time evolution of the radial star formation rate. To illustrate this we show the normalised star formation rate per unit surface area as a function of galactocentric radius in Figure 2. To match the chemical evolution models of Chiappini et al. (2001) for the Milky Way (with the understanding that our simulations are not constructed *a priori* to be perfect replicas of the Milky Way), we normalise the star formation rate to have a value of 1 $M_{\odot}$/Gyr/pc^2 at a galactocentric radius of 8 kpc.[14]

Each of the star formation rate profiles behave qualitatively like the classic inside-out chemical evolution models of Chiappini et al. (2001) and Mollá & Díaz (2005), in the sense of decreasing outwards from the inner to outer disks. An important systematic difference between these representative simulations is apparent though, at least at higher redshifts (1<z<2). Specifically, the gradient in the star formation rate per unit area is steeper at higher redshifts for the MUGS galaxies; it is not clear if this is symptomatic of a single difference between the MUGS and RaDES galaxies, or (more likely) a combination of factors including the star formation threshold, star formation efficiency, feedback schemes, and resolution of the respective simulations. Regardless, it is clear that *star formation is more centrally-concentrated in the MUGS sample at early stages in the formation of the disk which unsurprisingly leads to steeper abundance gradients in the early disk* (a point to which we return shortly).

3.2. Vertical Gradients

For completeness, as in Figs. 1 and 2, for g15784 (MUGS) and Apollo (RaDES), the mass-weighted vertical stellar abundance gradients in the simulations are presented in Figure 3. A 'solar neighbourhood' is defined for each simulation as being a 2 kpc annulus situated at a galactocentric radius of ∼2.5 disk scalelengths (column 5 of Table 1). These radial scalelengths were derived from exponential fits to the stellar surface density profiles.

Classic work from, for example, Marsakov & Borkova (2005, 2006) and Soubiran et al. (2008), and soon-to-be-released work using SDSS-SEGUE and RAVE datasets, show that vertical metallicity profiles can provide extremely effective tools for separating the thin disk from the thick disk. With ∼300−500 pc softening/grid cells, we do not resolve the thin-thick disk transition. Figure 3, shows the vertical gradient for the MUGS galaxy g15784 (orange) and the RaDES galaxy Apollo (purple), along with observational data for the Milky Way from Marsakov & Borkova (2005) and Marsakov & Borkova (2006). The two vertical lines show the respective resolutions of the MUGS and RaDES simulations.

The vertical metallicity gradients (in their respective 'solar neighbourhoods') for the 25 simulations analysed here are listed in column 7 of Table 1. We find little variation between the simulations in question, with the typical vertical gradient lying in the −0.05±0.03 dex/kpc range. Only Eos, Castor, and Krios lie outside this range, possessing somewhat steeper vertical abundance gradients. These three undergo the most extended late-time period of 'quiescent' evolution, as commented upon in Few et al., in prep.

At face value, the vertical gradients in [α/H][15] and [Fe/H] inferred from the simulations are consistent with the observed values seen in the thick disk of the Milky Way (∼−0.05 − ∼−0.08 dex/kpc). The vertical gradients in the Milky Way's thin disk, though, are consistently much steeper (where many authors find the thin disk gradient to be between ∼−0.25 − ∼−0.35 dex/kpc (e.g. Soubiran et al. 2008; Marsakov & Borkova 2006; Bartaši ūtė et al. 2003; Chen et al. 2003)) than the results we obtain from our simulations. Our spatial 'resolutions' range from ∼300−500 pc, and the results

[13] http://stev.oapd.inaf.it/cgi-bin/cmd_2.1

[14] For context, the 'normalised' and 'pre-normalised' star formation rate surface densities (at 8 kpc), for each of the simulations, are not dissimilar; the latter lie in the range ∼1−2 $M_{\odot}$/Gyr/pc^2, save for the (known) discrepant MUGS galaxy g24334 (which, pre-normalised, lies at ∼0.2 $M_{\odot}$/Gyr/pc^2, reflective of the fact that its stellar content is more dominated by its accreted component, rather than in situ star formation.

[15] Here, total metallicity is used as a proxy for α in the RaDES suite, while oxygen is used for the MUGS and GCD+ suites; magnesium is used in the observational datasets described by Marsakov & Borkova (2005, 2006).

appear compromised on vertical scales up to ∼2−3 resolution 'elements' - i.e., any putative 'thin' disk would be (not surprisingly) unresolved. In a chemical sense, these disks are too 'hot', in much the same way that their ISM and stellar populations are also kinematically hot (e.g. House et al. 2011).

On this issue of 'resolution', the global star formation rates reported are comparatively well converged as a function of resolution (Stinson et al. 2006, §5.2.4) The most notable change with increasing resolution is the addition of higher redshift populations, containing comparatively little mass, as earlier generations of halos are resolved. This is at least partially a result of star formation models largely being constrained to reproduce observed star formation rates.

The dependence of gradients on resolution though is far less predictable. At our current resolution we resolve sufficient substructure and disc dynamics to capture the salient physical mechanisms involved in migration. However, increasing resolution does resolve the physics behind migration processes better, but it also makes the diffusion model more localized. Equally importantly, it is not clear to what extent the numerous processes involved in migration will interact with one another as resolution is increased. Taking the alternative approach of lowering resolution makes processes less likely to be captured (particularly substructure-induced migration), so it is not clear that convergence happens in a simple fashion. Ultimately, a definitive answer on the impact of resolution on migration requires far higher resolution than we are currently able to achieve and future work is required to address this issue.

4. Evolution of the Radial Gradients

While there exist a handful of studies of radial abundance gradients at high redshift (Jones et al. 2010; Cresci et al. 2010; Yuan et al. 2011), the difficulties in obtaining high resolution data for likely Milky Way-like progenitors has meant that theoreticians have had very few constraints on their models; as noted earlier, inside-out galactic chemical evolution models can be constructed which recover the present-day gradients seen in the Milky Way, but they can take very different paths to get there. Some such models predict a steepening with time starting from initially inverted or flat gradients (e.g., Chiappini et al. (2001)), while others predict an initially negative gradient that flattens (e.g. Mollá & Díaz (2005)).

To make progress in this area, we now analyse the time evolution of the gradients within our 25 simulations, supplemented with two classical chemical evolution models, making fits radially at each timestep for which a clear disk could be identified. As the disk is continually growing and evolving, we examined each timestep visually, identifying the outer 'edge' using the cold gas and young stars as a demarcation point. It should be noted here that the kinematic decomposition used to identify 'disk stars' in § 3.1 and § 3.2 was not used for this component of our analysis.By working only with very young stars at 2−3 disk scalelengths, when fitting gradients at each timestep, kinematic decomposition of disk vs spheroid stars becomes unnecessary. Radial gradients were then derived by fitting typically from the outer edge of the disk to the inner part of the disk, where the inner point corresponds to the point at which the surface density profile deviates from an exponential. Again, as we are only using the stars formed in the previous 100 Myrs (B-stars) at a given timestep, the relevant disk (rather than star-forming bulge) regime is not difficult to identify.

In Figure 4, we show the time evolution of the radial gradient for our two 'fiducial' simulations: MUGS (g15784, upper panel) and RaDES (Apollo, lower panel). The gradients measured at each timestep are noted in the inset to each panel. Much steeper abundance gradients at high-redshift (z>1) are seen within the MUGS galaxy. Further, the offset in mean metallicity between the two, as already alluded to, can be traced to the manner in which chemistry was included in the version of GASOLINE employed (i.e., the assumption that Z≡O+Fe, which affects the mean metallicity, but not the gradient).

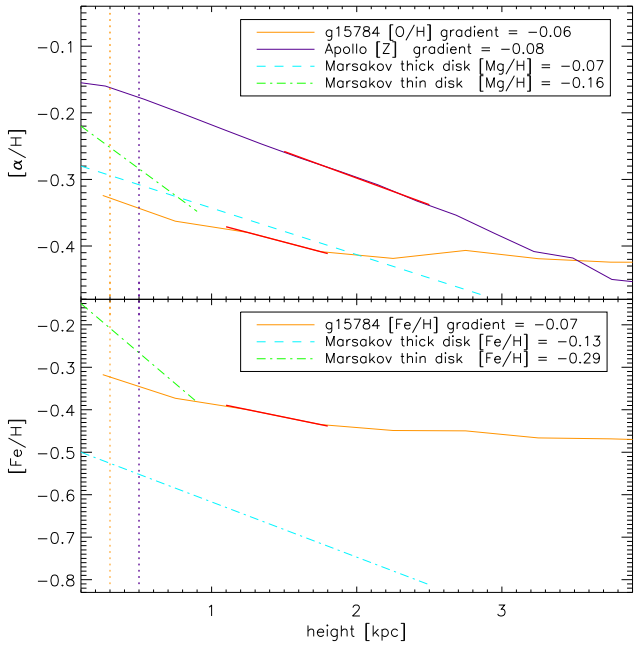

Fig. 3. The vertical gradients of disk stars in the simulations. The top panel shows the [Z] vertical gradient of Apollo (purple, grad = −0.08) with the [O/H] gradient of g15784 (orange, grad = −0.06) and observational data from Marsakov & Borkova (2005, 2006) of [Mg/H] gradients in the thin (blue, grad = −0.16) and thick (green, grad = −0.07) disk of the Milky Way. The lower panel shows the [Fe/H] gradients of the Marsakov & Borkova (2005, 2006) thin (grad = −0.29) and thick (grad =−0.13) disk data along with the g15784 (grad = −0.07) [Fe/H] gradient. Overplotted vertically are the softening length of the MUGS (orange) and the minimum grid size of the RaDES (purple) simulations. The bold red lines show the region used to calculate the gradient.

In Figure 5, we show the time evolution of the [Z] gradients for the 4 MUGS galaxies, the GCD+ galaxy (Gal1), the GRAPE-SPH galaxy (KN11), and the 19 RaDES galaxies. Importantly, we have also derived the time evolution of the predicted gradients for the chemical evolution models of Chiappini et al. (2001) and two of the Milky Way-like models of Mollá & Díaz (2005); with the Mollá & Díaz (2005) data, the fits to determine the gradient at each timestep evolved as they did in the hydrodynamical simulations. As the disk grew, the fits were made at larger radii, to exclude the central region. From the earliest timestep to the latest the fitted region shifts ∼3 kpc in radius (reflecting the growth of the disk over the timescales under consideration). The Chiappini et al. (2001) data were fit over the radial range 4 to 8 kpc at each timestep, reflecting the fewer relevant annuli available over which to make the fit. Chiappini et al. (2001) fit their gradients to the same chemical evolution models over a broader radial range (4−14 kpc), but our interests here are restricted to

the inner disks of these models, where the star formation density threshold is less important in shaping the metallicity gradient.

For the Mollá & Díaz (2005) models, we show a low-efficiency (28,8) and high-efficiency (28,2) example, (where model 28 corresponds to a circular velocity of ∼200 km/s and the efficiency factors correspond to the combined efficiency of molecular cloud formation and cloud-cloud collisions). The Chiappini et al. (2001) and, to a lesser extent, the high efficiency Mollá & Díaz (2005) models (at least since $z\sim1$) steepen with time.[16] Conversely, the RaDES sample (represented by the purple hatched region, which encompasses 1σ of the gradient values at a given redshift) shows a mild flattening with time, more in keeping with full time evolution of the high efficiency Mollá & Díaz (2005) model. The MUGS sample shows not only steeper gradients as a whole at $z>1$ (except for g24334, to which we return below), but also three of the four show the more significant degree of flattening alluded to in relation to Fig 4; this degree of flattening is more dramatic than that seen in any of the RaDES galaxies or the chemical evolution models (except for the low efficiency models of Mollá & Díaz (2005)).[17]

Shown also in Fig 5 are the typical gradients encountered in nearby isolated (Zaritsky et al. (1994); blue asterisk) and interacting (Kewley et al. (2010); red asterisk) disk galaxies (offset at z=0, for clarity, in Fig 5). The black asterisk at redshift $z\sim1.5$ corresponds to the recent determination of a steep metallicity gradient in a high-redshift grand design spiral by Yuan et al. (2011). While intriguing, it is important to bear in mind that one should not necessarily make a causal link between these disparate data points; until a statistical sample of high-redshift gradients has been constructed, linking the Yuan et al. (2011) point with those at low-redshift should be done with caution.

For this latter reason, we have also included one MUGS galaxy (g24334) in our analysis (red curve: Fig 5) that does not have a present-day gradient consistent with the typical late-type spiral. We chose to include it, in order for the reader to see one example of a disk which possesses a steep gas-phase abundance gradient at high-redshift, comparable in slope to the Yuan et al. (2011) observation, but one which does not evolve in time to resemble the shallower slopes seen in nature today. g24334 differs from the other MUGS galaxies, in the sense that the fraction of its stellar population born 'in situ', as opposed to 'accreted', is significantly lower. Further, its disk is less extended than the other Milky Way-analogs and its abundance gradient was derived at ∼0.5× disc scalelengths, where the gradient is more robust to interaction-induced flattening (e.g. Perez et al. 2011).

These differences are ultimately traced to the underlying treatment of star formation and feedback within the simulations; for example, the MUGS galaxies have a higher star formation threshold than the RaDES suite (1 cm^{-3} vs 0.1 cm^{-3}). As such, both the MUGS sample and the low efficiency models of Mollá & Díaz (2005) preferentially form stars in the inner disk where the densities are higher; the RaDES galaxies and the remaining chemical evolution models, with the lower threshold, have star formation occurring more uniformly throughout the early disk. Further, both MUGS and RaDES employ a standard blast-wave formalism for energy deposition into the ISM (Stinson et al. 2006), but the latter imposes a minimum blast wave radius of 2 grid cells, which means that ejecta is in some sense more "localised" in the MUGS simulations (for the same SN energy, the RaDES blast waves are ∼2−3× larger); distributing energy (and metals) on larger radial scales can result in a more uniform (i.e., flattened) metallicity distribution. The trend of Gal1 lies somewhat between the extremes of MUGS and RaDES, which can be traced to the fact that Gal1 uses a lower star formation threshold density (0.1 cm^{-3}), and almost negligible feedback, resulting in more localised metal enrichment. KN11 also lies very close to the MUGS fiducial (g15784) in terms of the temporal evolution of its abundance gradient; both employ high SNe feedback efficiencies, albeit on different spatial scales (a density-dependent blast wave radius in the case of g15784 and a fixed 1 kpc radius in the case of KN11) and with different star formation prescriptions (a 1 cm^{-3} star formation density threshold in the case of g15784 and an absence of a threshold for KN11). Note that although these hydrodynamical simulations experience different merger histories, the metallicity gradients are more affected by the recipe of sub-grid physics. This is highlighted by our large samples of simulations generated with different codes.

As detailed in § 2.5, Chiappini et al. (2001) use a two infall model; at early times the infall of primordial gas is rapid and independent of galactocentric radius, while at later times, gas is assumed to fall preferentially on the outer regions of the disk, causing a steepening of the gradient with time. The radial dependence of this disk infall timescale is fairly gentle (linear with increasing radius); on the other hand, Mollá & Díaz (2005) calculate the overall infall rate as a function of the mass distribution and rotation of the galaxy, and assume a much stronger radial dependence for the infall timescale. Specifically, the inner disk's infall timescale is much more rapid than that of Chiappini et al. (2001), while the outer disk's infall timescale is much longer. In combination, the gradient tends to flatten with time (particularly for their low efficiency models).

We find clear evidence of inside-out formation in the star formation profiles at different redshifts. Starting from an initially concentrated distribution, this flattens with time to the present-day, where star formation is more extended (and close to constant) over a large fraction of the disk (Fig 2). The radial dependence of star formation rate to infall rate sets the magnitude of the abundance gradient (Chiappini et al. 2001); a stronger radial dependence resulting in a steeper gradient. Such a configuration appears to come about naturally in the MUGS simulations, due in part to their higher star formation rate density threshold and perhaps the higher star formation efficiency and more localised chemical/energetic feedback. This contributes to the steeper gradients seen at early times in these simulations, relative to the other models. The RaDES galaxies behave more like the high

[16] The Chiappini et al. (2001) models have gradients which are mildly inverted at high-redshift (∼+0.02 dex/kpc at redshift $z\sim2$); this works in the same direction as the inverted gradients observed by Cresci et al. (2010) at $z\sim3$, albeit the gradients claimed by the latter are significantly more inverted (i.e., ∼+0.1 dex/kpc) than encountered in any of the simulations or chemical evolution models. It is important to remember though that the AMAZE/LSD samples at $z\sim3.3$ are (a) primarily Lyman-Break Galaxies with star formation rates (∼100−300 $M_\odot$/yr) well in excess of that expected for Milky Way-like progenitors, and are not likely ideal progenitors against which to compare these simulations or chemical evolution models, and (b) in none of the current simulations are we able to unequivocally identify stable rotationally-supported disks, like those compiled by AMAZE/LSD. We require targeted simulations with much higher resolution at high-redshift than we have access to here, and tuned to be more representative of high-redshift Lyman-break galaxies, before commenting further on this potentially interesting constraint.

[17] It is worth noting that no obvious trend is seen when comparing the field and group galaxies in the RaDES sample. This is perhaps attributable to our selection criteria; by removing strongly interacting galaxies (at or near a pericentre passage), the sort of systematic differences seen in the work of Rupke et al. (2010a,b); Perez et al. (2011), for example, would not be encountered here.

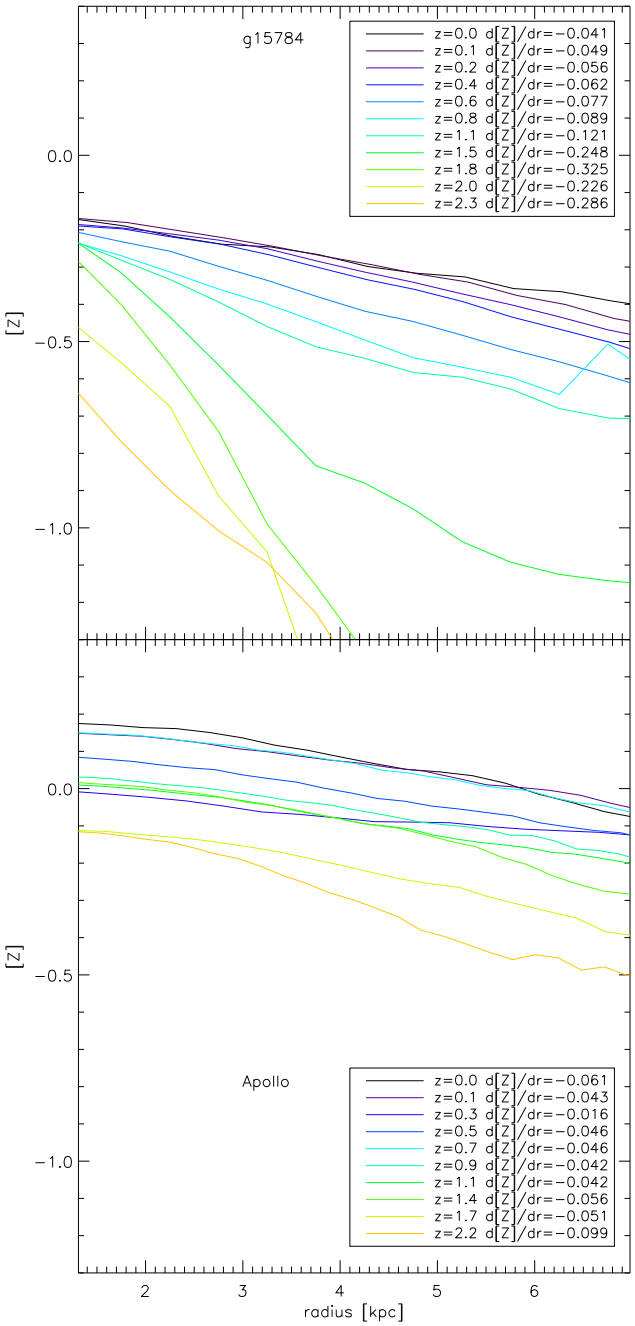

Fig. 4. The radial [Z] gradients of young stars in g15784 (top panel) and Apollo (bottom panel). The different colors correspond to different redshifts running from z=0 (black) to z=2.2 (orange), illustrating the time evolution of the abundance gradients in both simulations. Note the more dramatic flattening of the MUGS (g15784) relative to that of RaDES (Apollo). The fitted gradients were not done in an 'automated' fashion; we examined each timestep's surface density, kinematic, and abundance profiles, to take into account the growth of the disk and identify the 'cleanest' disk region within which to determine the gradient.

efficiency model of Mollá & Díaz (2005). It should be noted however that despite the significant differences seen in the early stages of these galaxies' evolution, the star formation distribution in the majority of these simulations is very similar at the present day.

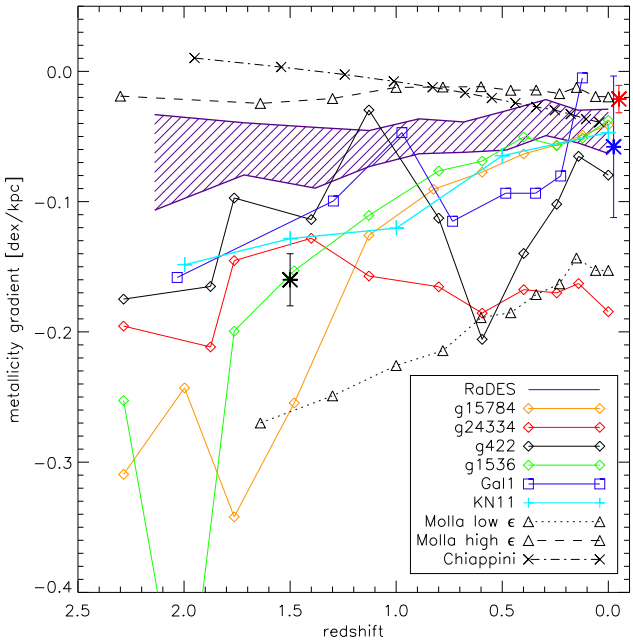

Fig. 5. The derived radial [Z] gradient as a function of redshift. Here, we have used 11 different redshifts and measured the radial gradient of the young stars (stars formed in the last 100 Myrs at each step) in the disk at that time. We examined the disks at each redshift, to determine the appropriate galactocentric radius over which to measure the gradients (see text for details). Four MUGS galaxies (g15784 (orange diamonds); g24334 (red diamonds); g422 (black diamonds); g1536 (green diamonds)) are shown, along with Gal1 (blue squares) from Rahimi et al. (2011), KN11 (cyan plus symbols) from Kobayashi & Nakasato (2011), and the 19 RaDES galaxies (denoted by the purple hatched area showing the region encapsulating 1σ of the gradients measured at a given redshift). The two chemical evolution models are overlaid for completeness: Chiappini (black dot dashed crosses), and Mollá high efficiency (black dashed triangles) and low effiency (black dotted triangles). The black asterisk corresponds to the result from one lensed grand design spiral at z~1.5 (Yuan et al. 2011), the blue asterisk to the typical gradient inferred in nearby spirals (Zaritsky et al. 1994), and the the red asterisk to the typical gradient seen in interacting disks (Kewley et al. 2010); these latter local points are offset slightly at z=0, for clarity.

5. Summary

This work provides evidence in support of the *imposed* inside-out disk growth paradigm adopted within chemical evolution models; this growth is a natural outcome of both Eulerian and Lagrangian hydrodynamical simulations of disk galaxy formation within a cosmological context. We have examined how this inside-out growth impacts on the magnitude and evolution of abundance gradients in these galaxies, using a suite of simulations and models which were calibrated to recover the present-day shallow gradients observed in late-type spirals. This is not meant to be a comprehensive, systematic, examination of sub-grid physics, in the vein of Wiersma et al. (2011), for example; instead, we have taken (in some sense) the 'best' Milky Way-like simulations from several groups, using different codes, different initial conditions, and different assembly histories, and conducted a 'blind' experiment on the outputs, to quantify *how* the

gradients evolved to the imposed boundary condition of a shallow present-day gradient. Our findings include the following:

1. All galaxy models and simulations described in this work exhibit inside-out formation of the disk with varying degrees of centrally-concentrated star formation at early times (Figure 2). The evolving radial star formation rate dependence directly influences the resulting metallicity gradient; put another way, the signature of the star formation profile is embedded within the gradient of the young stars at each timestep. This signature though is diluted on the timescale of a few Gyrs. This is reflected in the differing gradients at the present-day between old and young stars (Figure 1); young stars at high-redshift within the MUGS sample (and observationally, it would appear, tentatively) form with a steep metallicity gradient, while those same stars today (now, old) have a fairly flat metallicity gradient (see Pilkington & Gibson 2012).
2. Within the suite of 25 cosmological hydrodynamical simulations the derived vertical abundance gradients are comparable to those observed locally in the Milky Way's thick disk. The resolution is, however, not sufficient to discriminate between thin and thick disks.
3. The evolution of simulated metallicity gradients depends strongly on the choice of sub-grid physics employed and as such the magnitude and direction of its evolution depends critically upon the specific details of the recipes implemented. While it is difficult to disentangle the behaviour of the star formation profile *a priori*, it is clear that simulated galaxies with more centrally-concentrated star formation have initially steeper abundance gradients. These are more consistent with the (albeit limited) observation of high redshift normal Grand Design spiral galaxies (Yuan et al. 2011).
4. All the models and simulations tend to similar present-day abundance gradients, despite the diversity at earlier times, save for g24334 (which was chosen specifically in violation of the imposed shallow present-day gradient boundary condition, for illustrative purposes). In almost every case this requires the gradient to flatten with time, the exception being the chemical evolution model of Chiappini et al. (2001). This model starts with an initially positive gradient that is independent of its halo phase. The gradient then inverts to become negative, with a gradient similar to other chemical evolution models.
5. The diversity of the evolution of metallicity gradient is for the first time highlighted by our large sample of both hydrodynamical simulations and chemical evolution models. Our results indicate that observations of the metallicity gradient for disk galaxies at different redshifts and that for the different age populations in the Galaxy are key to reveal the formation processes of disk galaxies and better constrain the sub-grid physics implemented with all the codes sampled.

Future work in this area will see us employ a finer temporal cadence, in order to better track the precise influence of merger events on the abundance gradients (both the magnitude of the effect and the timescale for re-establishing a stable abundance gradient). This study will also yield a deeper understanding of how the non-linear processes of star formation and feedback influence systematic differences between the various simulations presented here. We are near completion of a major upgrade to RAMSES which will allow us to re-simulate the RaDES suite with a broad spectrum of chemical elements, including those from SNeII, SNeIa, and AGB stars. With ongoing and future large scale spectroscopic surveys and missions such as RAVE, APOGEE, SEGUE, HERMES, LAMOST, and Gaia, providing detailed information on the phase and chemical space signatures of the Milky Way and beyond, such a chemodynamical exploration will be both timely and critical for understanding the origin and evolution of abundances in galaxies, and their link to the underlying physics of galaxy formation.

Acknowledgements. The authors would like to acknowledge Romain Teyssier, for ongoing access to RAMSES. We also acknowledge the superb guidance and support of Stephanie Courty, Mario Abadi, and Patricia Sanchez-Blazquez, throughout the prepation of this work. The exceptional critique provided by the referee is particularly appreciated. KP and CGF acknowledge the support of STFC through its PhD Studentship programme (ST/F007701/1); visitor support (LMD, DK, MM) from the STFC (ST/G003025/1) is similarly acknowledged. BKG, CBB, and DK, acknowledge the support of the UK's Science & Technology Facilities Council (ST/F002432/1 & ST/H00260X/1). LMD acknowledges support from the Agence Nationale de la Recherche (ANR-08-BLAN-0274-01). RJT acknowledges support from NSERC, CFI, the CRC program, and NSRIT. BKG, KP, and CGF acknowledge the generous visitor support provided by Saint Mary's University. We thank the DEISA consortium, co-funded through EU FP6 project RI-031513 and the FP7 project RI-222919, for support within the DEISA Extreme Computing Initiative, the UK's National Cosmology Supercomputer (COSMOS), the University of Central Lancashire's High Performance Computing Facility, CfCA/NAOJ, JSS/JAXA, and the Shared Hierarchical Academic Research Computing Network (SHARCNET).

References

Abadi, M. G., Navarro, J. F., Steinmetz, M., & Eke, V. R. 2003, ApJ, 597, 21
Afflerbach, A., Churchwell, E., & Werner, M. W. 1997, ApJ, 478, 190
Asplund, M., Grevesse, N., Sauval, A. J., & Scott, P. 2009, ARA&A, 47, 481
Bailin, J., Kawata, D., Gibson, B. K., et al. 2005, ApJ, 627, L17
Bartaši ūtė, S., Aslan, Z., Boyle, R. P., et al. 2003, Baltic Astronomy, 12, 539
Carrera, R., Gallart, C., Aparicio, A., et al. 2008, AJ, 136, 1039
Chen, L., Hou, J. L., & Wang, J. J. 2003, AJ, 125, 1397
Chiappini, C., Matteucci, F., & Romano, D. 2001, ApJ, 554, 1044
Cooper, M. C., Tremonti, C. A., Newman, J. A., & Zabludoff, A. I. 2008, MNRAS, 390, 245
Cresci, G., Mannucci, F., Maiolino, R., et al. 2010, Nature, 467, 811
Dubois, Y. & Teyssier, R. 2008, A&A, 477, 79
Ferland, G. J., Korista, K. T., Verner, D. A., et al. 1998, PASP, 110, 761
Franx, M. & Illingworth, G. 1990, ApJ, 359, L41
Fu, J., Hou, J. L., Yin, J., & Chang, R. X. 2009, ApJ, 696, 668
Greggio, L. & Renzini, A. 1983, A&A, 118, 217
Haardt, F. & Madau, P. 1996, ApJ, 461, 20
House, E. L., Brook, C. B., Gibson, B. K., et al. 2011, MNRAS, 415, 2652
Iwamoto, K., Brachwitz, F., Nomoto, K., et al. 1999, ApJS, 125, 439
Jones, T., Ellis, R., Jullo, E., & Richard, J. 2010, ApJ, 725, L176
Karakas, A. I. 2010, MNRAS, 403, 1413
Kawata, D. & Gibson, B. K. 2003, MNRAS, 340, 908
Kawata, D., Gibson, B. K., & Windhorst, R. A. 2004, MNRAS, 354, 387
Kewley, L. J., Geller, M. J., & Barton, E. J. 2006, AJ, 131, 2004
Kewley, L. J., Rupke, D., Jabran Zahid, H., Geller, M. J., & Barton, E. J. 2010, ApJ, 721, L48
Klypin, A., Kravtsov, A. V., Bullock, J. S., & Primack, J. R. 2001, ApJ, 554, 903
Kobayashi, C. & Nakasato, N. 2011, ApJ, 729, 16
Kobayashi, C., Tsujimoto, T., & Nomoto, K. 2000, ApJ, 539, 26
Kobayashi, C., Umeda, H., Nomoto, K., Tominaga, N., & Ohkubo, T. 2006, ApJ, 653, 1145
Kormendy, J. & Djorgovski, S. 1989, ARA&A, 27, 235
Kroupa, P., Tout, C. A., & Gilmore, G. 1993, MNRAS, 262, 545
Maciel, W. J., Costa, R. D. D., & Uchida, M. M. M. 2003, A&A, 397, 667
Marigo, P., Girardi, L., Bressan, A., et al. 2008, A&A, 482, 883
Marsakov, V. A. & Borkova, T. V. 2005, Astronomy Letters, 31, 515
Marsakov, V. A. & Borkova, T. V. 2006, Astronomy Letters, 32, 376
Michel-Dansac, L., Lambas, D. G., Alonso, M. S., & Tissera, P. 2008, MNRAS, 386, L82
Mollá, M. & Díaz, A. I. 2005, MNRAS, 358, 521
Mollá, M., Ferrini, F., & Diaz, A. I. 1997, ApJ, 475, 519
Mollá, M., Hardy, E., & Beauchamp, D. 1999, ApJ, 513, 695
Monaghan, J. J. 1992, ARA&A, 30, 543
Nagamine, K. 2002, ApJ, 564, 73
Navarro, J. F., Abadi, M. G., Venn, K. A., Freeman, K. C., & Anguiano, B. 2011, MNRAS, 89

Nomoto, K., Iwamoto, K., Nakasato, N., et al. 1997, Nuclear Physics A, 621, 467
Okamoto, T., Nemmen, R. S., & Bower, R. G. 2008, MNRAS, 385, 161
Peletier, R. F., Davies, R. L., Illingworth, G. D., Davis, L. E., & Cawson, M. 1990, AJ, 100, 1091
Perez, J., Michel-Dansac, L., & Tissera, P. B. 2011, MNRAS, 417, 580
Persic, M., Salucci, P., & Stel, F. 1996, MNRAS, 281, 27
Pilkington, K. & Gibson, B. K. 2012, in Galactic Arachaeology: Near Field Cosmology and the Formation of the Milky Way, ed. W. Aoki, Astronomical Society of the Pacific Conference Series, in press
Prantzos, N. & Boissier, S. 2000, MNRAS, 313, 338
Queyrel, J., Contini, T., Kissler-Patig, M., et al. 2011, ArXiv e-prints
Rahimi, A., Kawata, D., Allende Prieto, C., et al. 2011, MNRAS, 725
Rahimi, A., Kawata, D., Brook, C. B., & Gibson, B. K. 2010, MNRAS, 401, 1826
Raiteri, C. M., Villata, M., & Navarro, J. F. 1996a, A&A, 315, 105
Raiteri, C. M., Villata, M., & Navarro, J. F. 1996b, Mem. Soc. Astron. Italiana, 67, 817
Rasera, Y. & Teyssier, R. 2006, A&A, 445, 1
Rupke, D. S. N., Kewley, L. J., & Barnes, J. E. 2010a, ApJ, 710, L156
Rupke, D. S. N., Kewley, L. J., & Chien, L. 2010b, ApJ, 723, 1255
Sánchez-Blázquez, P., Courty, S., Gibson, B. K., & Brook, C. B. 2009, MNRAS, 398, 591
Sánchez-Blázquez, P., Ocvirk, P., Gibson, B. K., Pérez, I., & Peletier, R. F. 2011, MNRAS, 415, 709
Scannapieco, C., Tissera, P. B., White, S. D. M., & Springel, V. 2008, MNRAS, 389, 1137
Shaver, P. A., McGee, R. X., Newton, L. M., Danks, A. C., & Pottasch, S. R. 1983, MNRAS, 204, 53
Shen, S., Wadsley, J., & Stinson, G. 2010, MNRAS, 407, 1581
Simpson, J. P., Colgan, S. W. J., Rubin, R. H., Erickson, E. F., & Haas, M. R. 1995, ApJ, 444, 721
Soubiran, C., Bienaymé, O., Mishenina, T. V., & Kovtyukh, V. V. 2008, A&A, 480, 91
Stinson, G., Seth, A., Katz, N., et al. 2006, MNRAS, 373, 1074
Stinson, G. S., Bailin, J., Couchman, H., et al. 2010, MNRAS, 408, 812
Sutherland, R. S. & Dopita, M. A. 1993, ApJS, 88, 253
Teyssier, R. 2002, A&A, 385, 337
Tosi, M. 1996, in Astronomical Society of the Pacific Conference Series, Vol. 98, From Stars to Galaxies: the Impact of Stellar Physics on Galaxy Evolution, ed. C. Leitherer, U. Fritze-von-Alvensleben, & J. Huchra, 299–+
van den Hoek, L. B. & Groenewegen, M. A. T. 1997, A&AS, 123, 305
van Zee, L., Salzer, J. J., Haynes, M. P., O'Donoghue, A. A., & Balonek, T. J. 1998, AJ, 116, 2805
Wadsley, J. W., Stadel, J., & Quinn, T. 2004, New Astronomy, 9, 137
Wiersma, R. P. C., Schaye, J., & Theuns, T. 2011, MNRAS, 732
Woosley, S. E. & Weaver, T. A. 1995, ApJS, 101, 181
Yuan, T.-T., Kewley, L. J., Swinbank, A. M., Richard, J., & Livermore, R. C. 2011, ApJ, 732, L14+
Zaritsky, D., Kennicutt, Jr., R. C., & Huchra, J. P. 1994, ApJ, 420, 87
Zolotov, A., Willman, B., Brooks, A. M., et al. 2010, ApJ, 721, 738